Magnetocardiography did not Uncover Electrically Silent Ischemia in an In-Silico Study Case

Danila Potyagaylo, Gunnar Seemann, Walther HW Schulze, Olaf Dössel

Institute of Biomedical Engineering, Karlsruhe Institute of Technology (KIT), Karlsruhe, Germany

Abstract

Over the last decades, the information content derived from cardiac electric and magnetic field measurements has been debated. Our co-workers Wilhelms et al. investigated electrically silent acute ischemia in human ventricles caused by occlusion of a coronary artery. In the present work, we extend the previous study by calculating associated magnetic fields produced by early stage acute ischemia with varying transmural extent. Multiscale computational simulations were performed for calculations of body surface potential maps (BSPM) and magnetocardiograms (MCG) on a magnetometer sensor matrix situated above the anterior chest wall. Depending on the ischemia size, the ST-segments of the simulated electrocardiograms (ECG) experienced depression for subendocardial cases and elevation for transmural ischemia. One intermediate extent resulted in a zero ST-segment which makes it diagnostically indistinguishable from the healthy case. Magnetic field calculations for this electrically silent ischemia also revealed no difference compared to the control case. Otherwise, both ECG and MCG signals during ST-segments showed either depression or elevation from zero line. In this simulation study, MCG did not deliver additional information to uncover electrically silent ischemia. For a general conclusion, further in-silico investigations with different ischemia shapes, sizes and positions should be performed and clinical studies with recordings of both ECG and MCG signals have to be conducted.

1. Introduction

Acute cardiac ischemia is caused by reduced blood supply due to occlusion of a coronary artery. In many cases, pathoelectrophysiological properties of the affected tissue result in severe ventricular arrhythmias that appear in two phases in the first 30 minutes of an acute ischemia [1]. The first phase, Phase 1a, lasts between 2 and 10 minutes and is associated with hyperkalemia, acidosis and hypoxia, resulting in reduced conduction velocity and action potential amplitude. These time-dependent effects lead to further classification: stage 1 (S1) is reached in minutes 5 to 7 of Phase 1a, stage 2 (S2) in minutes 10 to 12 [2]. The following Phase 1b lasts between 20 and 30 minutes after occlusion and is related to cellular electrical uncoupling.

Besides these temporal changes, ischemia undergoes spatial variations: immediately after coronary artery occlusion it often appears first on the subendocardium. In the absence of proper early management the subendocardial acute ischemia spreads transmurally toward the subepicardium.

Diagnosis of acute ischemia in 12-lead ECG is mainly based on changes during the ST-segment that are caused by injury currents flowing from healthy to affected tissue. Direction and strength of these currents are greatly influenced by ischemia extent and stage. Magnetocardiography (MCG) records the magnetic fields produced by the same bioelectric currents giving rise to ECG [3]. In comparison to ECG, MCG was shown to be more sensitive to tangential currents in the heart [4]. Furthermore, it can detect vortex-like sources, which are electrically silent, and thus deliver an information complementary to ECG [5, 6]. Thereby, computational simulations of electromagnetic fields generated by cardiac sources represent an essential step towards comprehensive understanding of underlying mechanisms and an improved early diagnosis.

2. Methods

Our co-workers Wilhelms *et al.* investigated acute electrically silent ischemia in the human ventricles caused by occlusion of a coronary artery in an in-silico model [7]. They introduced heterogeneous ischemic regions with varying transmural extent and analyzed the ECG effects of these ischemia at three stages (S1, S2, Phase 1b) during the first 30 minutes. As the primary goal of the current work was to investigate whether MCG contains information additional to ECG for cases of electrically silent ischemia, we restricted ourselves to the stage S1: For these, we reproduced five ischemia simulations and calculated the corresponding body surface potential maps (BSPM) as well as magnetic fields on a magnetometer sensor plane situated above the anterior chest wall.

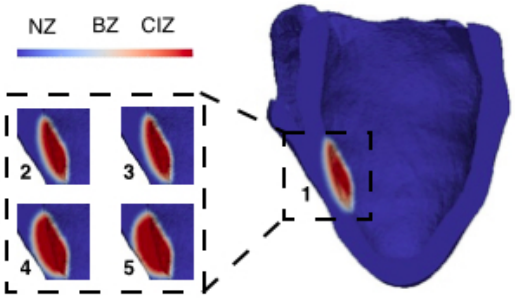

Figure 1: Ventricular model with spatially varying zone factors for simulation setups 1-5.

2.1. Modeling of acute ischemia and BSPM calculation

In our work, we used the Ten Tusscher ventricular cell model [8]. For modeling of acute ischemia, modified cell model paramenters from [7] were adopted. Excitation propagation and transmembrane voltages for a voxel-based heart model (0.4 mm resolution) of a healthy male volunteer were calculated with the parallel monodomain solver acCELLerate [9]. A rule-based endocardial stimulation profile imitating Purkinje fibers was used for simulating a normal ventricular activation sequence [10].

Similar to [7], an occlusion of the distal left anterior descending coronary artery was simulated. Regional heterogeneity of ischemia effects was modeled with the so-called zone factor (ZF). The normal zone (NZ) corresponding to healthy tissue was to set 0 and central ischemic zone (CIZ) to 1. Border zone (BZ) with varying hyperkalemia, acidosis and hypoxia dependent parameters was set to intermediate values [7]. The ischemic regions were modeled as ellipsoids and varied from subendocardial (setup 1) to almost transmural (setup 5) extent. In Fig. 1, the used ventricular model is visualized together with the simulation setup 1, image sections of varying ischemic transmural extents for simulation setups 2-5 are shown in the box to the left.

For numerical field calculations, a tetrahedral thorax model with a rule-based generated fiber orientation in the heart was used for solving the bidomain equations:

$$\nabla \cdot ((\sigma_e + \sigma_i)\, \nabla\phi) = -\nabla \cdot (\sigma_i \nabla V_m) \qquad (1)$$

where V_m are previously calculated transmembrane voltages, σ_e is the extracellular conductivity, σ_i the intracellular conductivity in the heart and ϕ are the electrical potentials to be computed at every geometry point. The calculations were done for the QRST-complex. The standard 12-lead ECG was derived from the BSPM, i.e. potentials on the torso surface.

2.2. Calculation of magnetic fields

The magnetic flux density B at the measurement points r is given by the Biot-Savart law:

$$B(r) = \frac{\mu_0}{4\pi} \int_\Omega \frac{J(r') \times (r - r')}{|r - r'|^3} d\Omega \qquad (2)$$

where J is the total current density at each source point r' and μ_0 the vacuum permeability.

The current density in the bidomain formulation reads:

$$J = -(\sigma_e + \sigma_i)\nabla\phi - \sigma_i \nabla V_m \qquad (3)$$

Whist the first term is due to Ohm's law, the second summand describes the impressed current density in the heart.

The magnetic field was calculated at 33 magnetometer sensors located in average 4 cm above the anterior chest wall. Afterwards, the signal was calculated in the direction normal to the sensor plane.

3. Results

In the present work, we performed computations of electromagnetic fields in a human body for a control case and 5 ischemia simulation setups with varying transmural extent during stage S1. In line with the previous findings of our colleagues, the ECG signals in the precordial lead V_4 showed the most prominent changes in the 12-lead ECG. Resulting electrocardiograms at V_4 are presented in Fig. 3.

While the QRS-complexes from the acute ischemia setups were very similar to the control case, major changes arose in the ST-segment and T-wave. For the simulation setups 1 and 2, a slight ST-segment depression was observed. The ischemia corresponding to setup 3 was almost indistinguishable from the control case, whereas the ischemia of greater transmural extent showed a clear ST elevation. For these setups, the T-wave started earlier and had a larger amplitude than the control case.

In Fig. 2 (upper row) the BSPM for the time instance $t = 200$ ms, which corresponds to the ST-segment, of all 6 cases are visualized on the torso surface. For the control case a slight elevation near the V_4 lead was observed. Whereas the BSPM for setup 3 was almost identical to the control case, setups 4 and 5 featured a distinct elevation of this region.

In order to evaluate the differences in magnetic fields produced from healthy and ischemic source configurations, we visualized the MCG signals on the sensor plane at the same time instance $t = 200$ ms (see Fig. 2, lower row). Note that the MCG maps for the control case and setup 3 showed a very similar pattern, whilst other ischemia setups revealed more distinct positive and negative pole location shifts. The correlation coefficients between the healthy case and setups 1-5 were 92.79 %, 92.52 %,

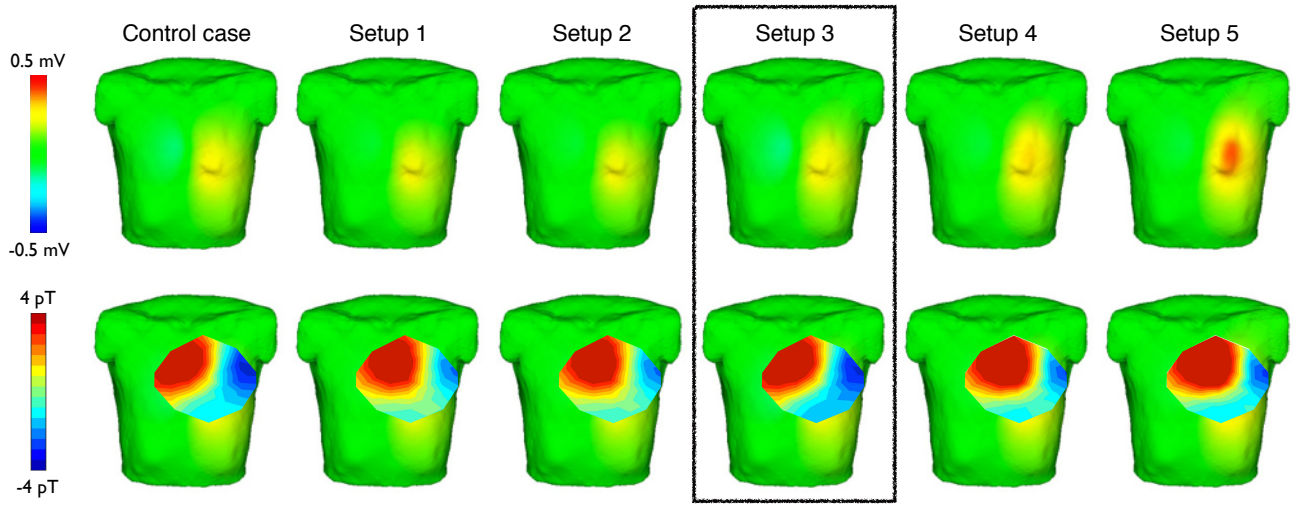

Figure 2: BSPM (upper row) and MCG (lower row) of the control case and ischemia simulation setups 1-5.

99.57 %, 89.02 % and 86.9 %, respectively. In Fig. 4 and 5 MCG signals minima and maxima for all sensors for the simulated heart cycle are plotted. While the QRS-complexes of the control and ischemic cases stayed very similar, the most prominent changes arose during the ST-segment and T-wave time intervals. The largest amplitude difference was achieved for setups 4 and 5.

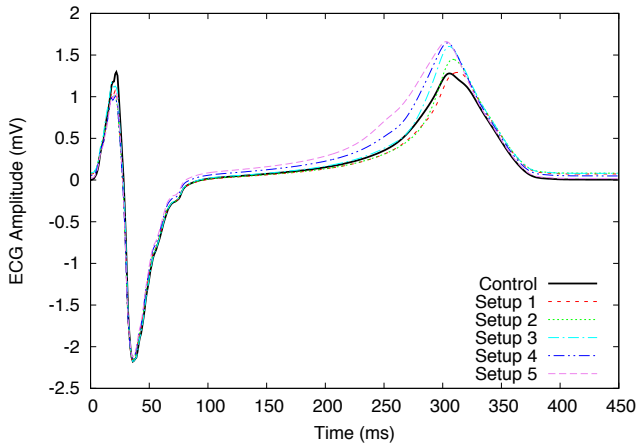

Figure 3: ECG at Wilson V4 lead for the control case and simulation setups 1-5.

4. Discussion and conclusions

In the last decades there have been discussions and arguments concerning additional information content provided by magnetic field measurements. One possible application of MCG could be detection of electrically silent ischemia that mostly manifests in the ST-segment shift in the ECG.

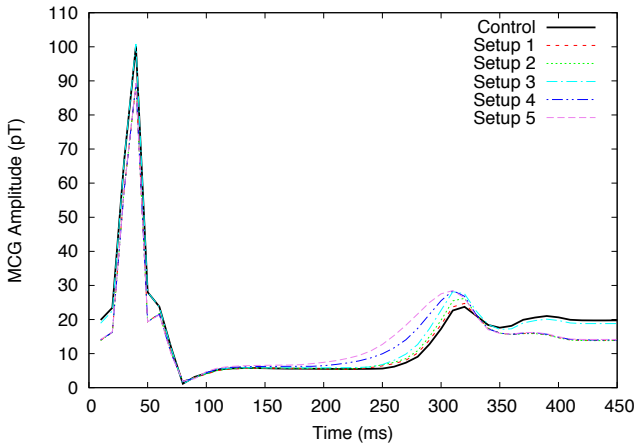

Figure 4: Largest positive MCG signal for the control case and simulation setups 1-5.

Although the BSPM improve the detection rate compared to the standard 12-lead ECG [11], some cases are still indistinguishable from the healthy one.

The complementary nature of MCG and ECG for patients with ischemic heart disease was demonstrated by Lant *et al.* in [6]. In many clinically reported cases, MCG showed morphological changes in the QRS-complex, ST-segment shifts and T-wave alterations resembling those in the ECG [12]. In several studies for acute ischemia patients and patients with myocardial infarction showing non-ST-changes, MCG was able to detect the heart disease [13,14].

In contrast to these findings, we did not observe any improvement in the detection of ischemia with no ST-shift in the ECG. In our work, the compensation effects leading to non-ST-segment shift and no changes in MCG could prob-

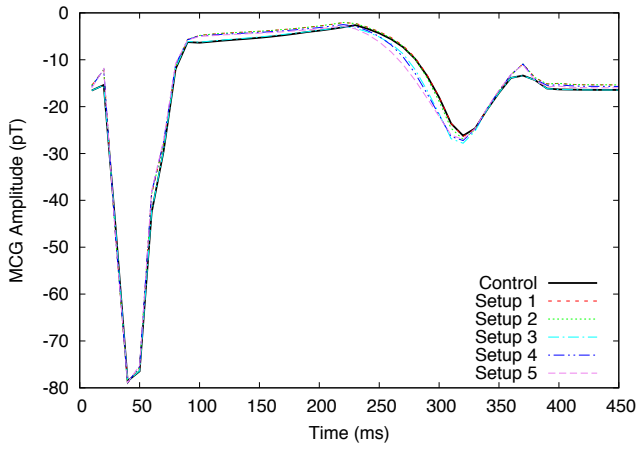

Figure 5: Largest negative MCG signal for the control case and simulation setups 1-5.

ably be caused by the simplified elliptical form of the simulated ischemia. Therefore, further ischemia simulation studies with varying geometrical forms, sizes and locations are mandatory for evaluation of MCG performance for ischemia patients [15]. Furthermore, it should also be tested in simulation and clinical studies whether a combination of both approaches and application of new spatio-temporal ECG-MCG markers would improve detection rates for non ST shift ischemia patients.

Acknowledgements

Authors would like to thank Matti Stenroos and Ville Mäntynen for providing the location of the used MCG sensor array.

References

[1] Cascio WE, Yang H, Muller-Borer BJ, Johnson TA. Ischemia-induced arrhythmia: the role of connexins, gap junctions, and attendant changes in impulse propagation. J Electrocardiol 2005;38(4 Suppl):55–59.

[2] Rodriguez B, Tice BM, Eason JC, Aguel F, Trayanova N. Cardiac vulnerability to electric shocks during phase 1a of acute global ischemia. Heart Rhythm the Official Journal of the Heart Rhythm Society 2004;1(6):695–703.

[3] Takala P, Hänninen H, Montonen J, Mäkijärvi M, Nenonen J, Oikarinen L, Simelius K, Toivonen L, Katila T. Magnetocardiographic and electrocardiographic exercise mapping in healthy subjects. Annals of biomedical engineering 2001; 29(6):501509.

[4] Mantynen V, Konttila T, Stenroos M. Investigations of sensitivity and resolution of ECG and MCG in a realistically shaped thorax model. Physics in Medicine and Biology 2014;59(23):7141–7158.

[5] Roth BJ, Wikswo JPJ. Electrically silent magnetic fields. Biophys J 1986;50(4):739–745.

[6] Lant J, Stroink G, tenVoorde BJ. Complementary nature of electrocardiographic and magnetocardiographic data in patients with ischemic heart disease. Journal of Electrocardiology 1990;23(4):315–322.

[7] Wilhelms M, Dössel O, Seemann G. In silico investigation of electrically silent acute cardiac ischemia in the human ventricles. IEEE Trans on Biomed Eng 2011;58(10):2961–2964.

[8] ten Tusscher KHWJ, Panfilov AV. Alternans and spiral breakup in a human ventricular tissue model. American Journal of Physiology Heart and Circulatory Physiology 2006;291(3):H1088–100.

[9] Seemann G, Sachse FB, Karl M, Weiss DL, Heuveline V, Dössel O. Framework for modular, flexible and efficient solving the cardiac bidomain equation using PETSc. Mathematics in Industry 2010;15(2):363–369.

[10] Keller DU, Weber FM, Seemann G, Doessel O. Ranking the influence of tissue conductivities on forward-calculated ecgs. IEEE Trans on Biomed Eng 2010;57(7):1568–1576.

[11] McClelland AJJ, Owens CG, Menown IBA, Lown M, Adgey AAJ. Comparison of the 80-lead body surface map to physician and to 12-lead electrocardiogram in detection of acute myocardial infarction. The American Journal of Cardiology 2003;92(3):252–257.

[12] Osterhues HH, Hombach V, Moss AJ. Advances in noninvasive electrocardiographic monitoring techniques, volume 229. Springer Science & Business Media, 2000.

[13] Park JW, Hill P, Chung N, Hugenholtz P, Jung F. Magnetocardiography predicts coronary artery disease in patients with acute chest pain. Annals of noninvasive electrocardiology 2005;10(3):312323.

[14] Kyoon Lim H, Kim K, Lee YH, Chung N. Detection of non-ST-elevation myocardial infarction using magnetocardiogram: New information from spatiotemporal electrical activation map. Annals of medicine 2009;41(7):533546.

[15] Loewe A, Schulze WHW, Jiang Y, Wilhelms M, Luik A, Dössel O, Seemann G. ECG-based detection of early myocardial ischemia in a computational model: Impact of additional electrodes, optimal placement, and a new feature for ST deviation. BioMed Research International Article 2014;ID 530352:1–11.

Address for correspondence:

Danila Potyagaylo
Institute of Biomedical Engineering, KIT,
Fritz-Haber-Weg 1, 76131 Karlsruhe, Germany
publications@ibt.kit.edu